

Visible-Light-Driven Nitrogen-doped Carbon Quantum Dots/CaTiO₃ Composite Catalyst with Enhanced NO Adsorption for NO Removal

Jiaoyang Wang, Fuman Han, Yongfang Rao, Tafeng Hu, Yu Huang, Jun-ji Cao, and Shun Cheng Lee

Ind. Eng. Chem. Res., **Just Accepted Manuscript** • DOI: 10.1021/acs.iecr.8b01731 • Publication Date (Web): 20 Jul 2018

Downloaded from <http://pubs.acs.org> on July 24, 2018

Just Accepted

“Just Accepted” manuscripts have been peer-reviewed and accepted for publication. They are posted online prior to technical editing, formatting for publication and author proofing. The American Chemical Society provides “Just Accepted” as a service to the research community to expedite the dissemination of scientific material as soon as possible after acceptance. “Just Accepted” manuscripts appear in full in PDF format accompanied by an HTML abstract. “Just Accepted” manuscripts have been fully peer reviewed, but should not be considered the official version of record. They are citable by the Digital Object Identifier (DOI®). “Just Accepted” is an optional service offered to authors. Therefore, the “Just Accepted” Web site may not include all articles that will be published in the journal. After a manuscript is technically edited and formatted, it will be removed from the “Just Accepted” Web site and published as an ASAP article. Note that technical editing may introduce minor changes to the manuscript text and/or graphics which could affect content, and all legal disclaimers and ethical guidelines that apply to the journal pertain. ACS cannot be held responsible for errors or consequences arising from the use of information contained in these “Just Accepted” manuscripts.



Visible-Light-Driven Nitrogen-doped Carbon Quantum Dots/CaTiO₃ Composite Catalyst with Enhanced NO Adsorption for NO Removal

Jiaoyang Wang¹, Fuman Han¹, Yongfang Rao^{1,3*}, Tafeng Hu³, Yu Huang^{2,3*}, Jun-ji Cao^{2,3}, Shun cheng Lee⁴

1. Department of Environmental Science and Engineering, Xi'an Jiaotong University, Xi'an 710049, PR China
2. Key Laboratory of Aerosol Chemistry and Physics, Institute of Earth Environment, Chinese Academy of Sciences, Xi'an 710075, China.
3. State Key Lab of Loess and Quaternary Geology (SKLLQG), Institute of Earth Environment, Chinese Academy of Sciences, Xi'an 710075, China.
4. Department of Civil and Environmental Engineering, The Hong Kong Polytechnic University, Hong Kong, China

ABSTRACT: Nitrogen oxides (NO_x) have attracted extensive concerns as a secondary aerosol precursor in recent years. Solar-induced photocatalytic oxidation is a promising strategy for of NO_x removal nowadays. In this contribution, nitrogen-doped carbon quantum dots (N-CQDs)/CaTiO₃ composite was synthesized using a facile hydrothermal process. The incorporation of N-CQDs to CaTiO₃

* To whom correspondence should be addressed. Email: yf rao@mail.xjtu.edu.cn (Yongfang Rao); huangyu@ieecas.cn (Yu Huang)

1
2
3 facilitates the transfer of electrons and divorce of photo-generated carriers. NO
4
5
6 temperature-programmed desorption (NO-TPD) demonstrated that the presence of
7
8 N-CQDs was conducive to the NO adsorption in comparison with the pristine CaTiO₃.
9
10 The composite catalyst demonstrated much better photocatalytic performance than
11
12 CaTiO₃ and P25 did in regard to gaseous NO removal and NO₂ selectivity under
13
14 visible light irradiation. Both $\cdot\text{O}_2^-$ and $\cdot\text{OH}$ are believed to make a major
15
16 contribution to NO removal. The role of N-CQDs was unraveled in the photocatalytic
17
18 reaction of NO elimination over N-CQDs/CaTiO₃ samples. This study provides an
19
20 insight into the composite catalyst N-CQDs/CaTiO₃ in photocatalytic reactions and
21
22 applications.
23
24
25
26
27
28
29
30
31
32
33
34
35
36
37
38
39
40
41
42
43
44
45
46
47
48
49
50
51
52
53
54
55
56
57
58
59
60

1 . INTRODUCTION

In the recent decades, the tremendous boost in energy consumption has induced significant NO_x concentration enhancement in the atmosphere in China¹⁻³. Nitrogen oxides (NO_x) were reported to be germane to haze events which have received extensive concerns as a secondary aerosol precursor⁴⁻⁶. Therefore, the diminution of NO_x concentration is pressing in the atmosphere. Typical deNO_x technologies such as three-way catalysis and selective catalytic reduction entail high temperature and reductants, rendering the elimination of NO_x economically unfeasible at parts per billion (ppb) level in the air⁷⁻⁹.

Solar-driven photocatalysis is an attractive alternative for NO_x removal at ppb level¹⁰⁻¹². Photocatalytic oxidation can convert NO to nitrate, while the generation of uninvited NO₂ may also be expected. Therefore, both high removal efficiency of NO and selectivity towards the formation of nitrate are equally crucial.

In recent years, perovskite-type oxides have gained increasing attention as functional materials because of its inimitable physical and chemical properties¹³⁻¹⁶. The typical structural formula of perovskite-type oxides is ABO₃, in which A indicates a rare or alkaline earth metal and B is occupied by a transition metal. Moreover, titanate perovskite ABO₃ (A=Ca, Sr, Ba, *etc.*) with high photo and thermal stability are reported as one of the promising materials for photocatalytic processes¹⁷. Among titanate perovskite-type oxides, CaTiO₃ with appropriate conduction band (CB) and valence band (VB) position, has attracted growing attention in the last decades¹⁸⁻²⁰. Unfortunately, its high band gap energy (3.5eV) confines its practical

1
2
3 application²¹. In order to effectively utilize solar energy, efforts such as metal doping
4
5 have been devoted to extend the optical response of CaTiO₃ into the visible spectral
6
7 range²². Unfortunately, metal doping may change the band structure of CaTiO₃,
8
9 leading to the variation of the potential of CB and VB, which may not be encouraging
10
11 for the generation of hydroxyl or superoxide radical. The introduction of quantum
12
13 dots can offer a possibility to extend the photo response of CaTiO₃ into visible light
14
15 range without changing its band structure.
16
17
18
19

20
21 Carbon quantum dots (CQDs), a new type of carbon nanomaterial sized smaller
22
23 than 10 nm, have attracted increasing attention in the photocatalysis realm due to their
24
25 excellent optical properties, chemical inertness, eco-friendliness, upconversion
26
27 photoluminescence and conjugated π structure which allows them to be electron
28
29 transporters and acceptors²³⁻²⁸. However, the CQDs usually show low fluorescence
30
31 quantum yields²⁹. Nitrogen doping can lower the work function, encourage charge
32
33 delocalization, and efficiently promote the electron-transfer capability of CQDs^{30,31}.
34
35 It was also reported nitrogen doping could increase fluorescence quantum yields of
36
37 CQDs²⁹. Owing to their photochemical properties, electrocatalytic activity,
38
39 biocompatibility and ability to reduce the work function of CQDs, the N-CQDs
40
41 showed much better performance than CQDs³²⁻³⁴. Zhang *et al*³¹ reported that
42
43 N-CQDs/TiO₂ composites have two times higher than P25 in visible light activity and
44
45 Wei *et al*³⁵ thought that the activity of TiO₂ for hydrogen evolution under solar
46
47 sunlight can be enhanced with the addition of N-CQD.
48
49
50
51
52
53
54
55
56
57
58
59
60

1
2
3 This work presents a N-CQDs/CaTiO₃ composite prepared by a simple
4 hydrothermal method. Comprehensive characterizations of the as-prepared catalysts
5 were conducted. We illuminated the roles of N-CQDs in the enhanced photocatalytic
6 activity of N-CQDs/CaTiO₃ and proposed the possible photocatalytic mechanisms. It
7 is the first time for N-CQDs/CaTiO₃ composites to be used in the photocatalytic
8 removal of NO_x.
9
10
11
12
13
14
15
16
17
18

19 **2. EXPERIMENTAL**

20
21
22 **2.1. Preparation of N-CQDs.** A simple hydrothermal method was applied to
23 prepare N-CQDs. Briefly, 3 g citric acid monohydrate (guarantee reagent, Sinopharm)
24 and 3 g urea (analytical grade reagents, Sinopharm) were first dissolved in 10 mL
25 deionized water and then the transparent solution was dispensed into a 50 mL
26 Teflonlined stainless steel autoclave which was heated at 180 °C for 4.5 h. After the
27 autoclave being cooled to room temperature, the dark green liquid was collected as
28 N-CQDs.
29
30
31
32
33
34
35
36
37
38

39 **2.2. Synthesis of N-CQDs/CaTiO₃ Composites.** The N-CQDs/CaTiO₃ was
40 synthesized by dosing predetermined N-CQDs amount into CaTiO₃ precursor solution
41 which suffered further solvothermal treatment. In particular, 2 mL 1 mol/L Ca(NO₃)₂·
42 4H₂O (analytical grade reagents, Sinopharm) were dissolved in 37 mL PEG-200
43 (polyethylene glycol, chemical purity, Sinopharm) and then 0.7 mL Tetrabutyl titanate
44 [titanium n-butoxide, Ti(OC₄H₉)₄, TNB] (chemical pure, Sinopharm) was dosed into
45 this solution being stirred vigorously. The 1.76 g of NaOH (chemical purity,
46 Sinopharm) was added into the obtained colloidal solution under continuous stirring
47
48
49
50
51
52
53
54
55
56
57
58
59
60

1
2
3 as a mineralizer. Subsequently, a predetermined dose of N-CQDs solution was
4 dispensed into the above solution, and the obtained suspension liquid was then
5
6 relocated to a 50 mL Teflonlined stainless steel autoclave which was heated at 180 °C
7
8 for 15 h. After the autoclave being cooled naturally to ambient temperature, the white
9
10 and yellow samples were collected and washed using dilute acetic acid, deionized
11
12 water and ethanol, sequently. The samples were eventually dried overnight at 60°C.
13
14 The N-CQDs/CaTiO₃ composites synthesized by varying the N-CQDs solution dose
15
16 of 0.1, 0.3, 0.5 mL were labeled as 1-N-CQDs/CaTiO₃, 3-N-CQDs/CaTiO₃, and
17
18 5-N-CQDs/CaTiO₃, respectively.
19
20
21
22
23
24

25 **2.3. Characterization.** The crystal structure of as-prepared catalysts was
26 analyzed using X-ray diffractometer (PANalytical X' Pert PRO) with a scan range of
27
28 20-80° (2θ) at a scan rate of 0.05°/s. Fouriertransform infrared spectroscopy (FT-IR)
29
30 was conducted on a Magna-IR 750 spectrometer (USA) in a range of 450-2000 cm⁻¹.
31
32 X-ray photoelectron spectroscopy (XPS; Physical Electrons Quantum2000 Scanning
33
34 Esca Microprob), scanning electron microscopy (SEM, JEOL JSM-6490) and
35
36 Transmission electron microscopy (TEM, JEOL JEM-2100HRCM-120) were utilized
37
38 to analyze chemical state, morphology and elemental distribution, and crystalline
39
40 structure, respectively. The N₂ adsorption/desorption isotherms which can be measured
41
42 at 77 K with an ASAP 2020 (Micromeritics Instrument Corp, U.S.A) were recorded in
43
44 order to determine the BET surface area of the as-synthesized catalysts. Moreover, the
45
46 reflectance spectra of the catalysts were characterized within a range of 200-800 nm
47
48 using a Varian Cary 100 Scan UV-vis system.
49
50
51
52
53
54
55
56
57
58
59
60

1
2
3
4 Themogravimetric Analysis (TG) was performed from 25 to 800 °C on a
5
6 Simultaneous Thermal Analysis instrument (STA 449F5) under nitrogen gas at a flow
7
8 rate of 30 mL/min. A chemisorption analyzer (BJbuilder, PCA 1200, China) was used
9
10 for Temperature programmed desorption (TPD): 50 mg of samples was pretreated by
11
12 N₂ at 300 °C for 30 min with a constant heating rate of 10 °C/min to eliminate surface
13
14 pollutants. After cooling to room temperature, the catalyst will be exposed in NO for
15
16 30 min. Once equilibrated, the sample was placed in the He atmosphere with a heating
17
18 rate of 10 °C/min to 800 °C to allow desorption of NO. Electron spin resonance
19
20 spectroscopy (ESR, ER200-SRC, Bruker, Germany) were applied to determine active
21
22 oxygen species generated during photocatalytic process with 5,5 '
23
24 -dimethyl-1-pyrroline-N-oxide (DMPO) solution as an adduct agent. Deionized water
25
26 and methanol were used as solvents for the identification of DMPO-•OH and DMPO-
27
28 •O₂⁻, respectively, under the irradiation of 420 nm visible light. The yield of
29
30 intermediate and final products such as nitrate and nitrite ions, was quantified by Ion
31
32 Chromatograph (IC, Dionex-600, USA) equipped with an IonPac AS14A column.
33
34
35
36
37
38
39

40 The photocurrent measurement of as-synthesized samples was similar to our
41
42 previous studies³⁶.
43
44

45 **2.4. Photocatalytic Activity Test.** The photocatalytic activities of CaTiO₃ and
46
47 N-CQDs/CaTiO₃ with different N-CQDs dose were examined in terms of NO
48
49 removal. The chamber for testing was fabricated with stainless steel and covered by
50
51 quartz glass in accordance with the ISO 22197-1 standard. A 300 W xenon lamp
52
53 (microsolar 300, Perfectlight, China) was used to offer the visible light (>420 nm)
54
55
56
57
58
59
60

1
2
3 with UV light being removed. For testing, an aqueous suspension with 0.1 g catalyst
4
5 was coating onto a glass dish (diameter = 12 cm) by pretreating at 70 °C for few hours
6
7 to completely remove the water.
8
9

10 The initial NO concentration was 400 ppb and the flow rate were 3 L/min. A
11
12 chemiluminescence NO analyzer (Model 42c, Thermo Environmental Instruments
13
14 Inc, Franklin, MA, USA) was used to measure the concentration of NO with a
15
16 sampling 0.7 L/min. The photocatalytic reaction using P25 as a catalyst was also
17
18 conducted under identical conditions as a comparison.
19
20
21
22

23 The removal efficiency (η) of NO was calculated as $\eta (\%) = (1-C/C_0) \times 100$, where
24
25 C is the NO residual during NO photocatalytic degradation, ppb; and C_0 is NO initial
26
27 concentration (ppb). NO_2 concentration was simultaneously measured during the
28
29 photocatalytic process, and its yield can be obtained by using the equation ΔNO_2
30
31 (ppb) = $C - C_0$, in which C represents the NO_2 concentration after reaction (ppb); and
32
33 the C_0 is NO_2 initial concentration. Finally, we can use the equation NO_2 conversion
34
35 rate = $\Delta\text{NO}_2/(C-C_0)$ in which C represents the initial NO concentration, the C_0
36
37 represents the NO concentration after reaction to represent the NO_2 conversion ration
38
39 in the whole experiment.
40
41
42
43
44
45

46 **3. RESULTS AND DISCUSSION**

47
48 **3.1 Phase structure and chemical compositions.** The crystal phase of
49
50 as-synthesized CaTiO_3 and N-CQDs/ CaTiO_3 composites were characterized via XRD.
51
52 As shown in Figure 1, all diffraction peaks of the tested samples can be ascribed to
53
54 pure orthorhombic CaTiO_3 ($a = 5.38290 \text{ \AA}$, $b = 7.64530 \text{ \AA}$, $c = 5.44580 \text{ \AA}$, JCPDS
55
56
57
58
59
60

1
2
3 no.76-2400). The diffraction peaks at 2θ values of 23.1° , 33.1° , 47.4° , 59.2° , 69.4°
4
5 corresponds to the (101), (121), (202), (321) and (242) reflection respectively.
6
7
8 However, the characteristic peak of N-CQDs (approximately 25.6°)³⁷ was not detected
9
10 in N-CQDs/CaTiO₃ composites, which may be on account of the low content and
11
12 highly-scattered N-CQDs in these samples. Moreover, in the case of N-CQDs/CaTiO₃
13
14 catalysts, no shift of the diffraction peaks of CaTiO₃ was observed, indicating that the
15
16 phase structure of CaTiO₃ remained stable in the presence of N-CQDs during the
17
18 synthesis process.
19
20
21
22

23 FT-IR spectra were measured to further confirm the existence of carbon quantum
24
25 dots in the complex structures of N-CQDs/CaTiO₃. As demonstrated in Figure 2a,
26
27 besides the peaks coming from CaTiO₃, a characteristic peak located at 1330 cm^{-1}
28
29 corresponding to the C-O-C²⁷ was observed, suggesting the existence of CQDs in the
30
31 composite catalysts.
32
33
34

35 To test if the nitrogen was doped into the carbon quantum dots, XPS was conducted
36
37 over the N-CQDs. As illustrated in Figure 2b, the survey spectrum confirms that the
38
39 CQDs sample contains N element, indicating nitrogen was successfully doped into the
40
41 CQDs.
42
43
44

45 **3.2 Morphology.** SEM and TEM were utilized to delineate the micrograph and
46
47 crystallographic structure of the 3-N-CQDs/CaTiO₃ material (See Figure 3). As
48
49 demonstrated in Figure 3a-c, the lattice fringe spacing of 0.383 nm derives from the
50
51 (101) plane of the orthorhombic-structured CaTiO₃ while the lattice fringe spacing of
52
53
54
55
56
57
58
59
60

1
2
3 roughly 0.209 nm is attributed to the (010) lattice planes of the hexagonal graphitic
4 carbon³².
5
6

7
8 The SEM images of 3-N-CQDs/CaTiO₃ sample were illustrated in Figure 3d and
9 Figure S1. The cubic particles with a size ranging from 500 nm to 1 μm can be
10 observed. As demonstrated in Figure S1, after being modified by suitable N-CQDs,
11 CaTiO₃ maintains the original shape. However, with the addition of 0.5 mL N-CQDs,
12 the agglomeration can be observed, implying overdose N-CQDs can change the
13 morphology of CaTiO₃. With the aim of investigating the elemental dispersion over
14 the N-CQDs/CaTiO₃ composite, EDX mapping was recorded and shown in Figure
15 3e-h. The result suggests that Ca (green), Ti (blue), O (purple), N (yellow) elements
16 are distributed evenly on the surface of sample. The sparse presence of N in
17 comparison with other elements provided cogent evidence for the distribution of
18 N-CQDs on the surface of CaTiO₃. It can be concluded that N-CQDs/CaTiO₃
19 composite was successfully synthesized.
20
21
22
23
24
25
26
27
28
29
30
31
32
33
34
35
36
37

38 **3.3 Textural, optical, electric and adsorption properties of samples.** The
39 specific surface area of CaTiO₃ was 13.0 m²/g, twice that of 3-N-CQDs/CaTiO₃ (6.4
40 m²/g), indicating the addition of N-CQDs reduced the BET surface area of CQDs (See
41 Table S1). The agglomeration was observed with the introduction of N-CQDs as
42 demonstrated in Figure S1, justifying the reduction of BET surface area of CaTiO₃
43 with the presence of N-CQDs.
44
45
46
47
48
49
50
51

52 In the presence of N-CQDs, the composite's absorption spectra exhibit an apparent
53 red shift, where the absorption edge extends to the visible region (See Figure 4a).
54
55
56
57
58
59
60

1
2
3 Furthermore, such a red shift hinges on the N-CQDs content. Pure CaTiO₃ can only
4 absorb UV light (<368 nm), based on which its band gap can be calculated to be 3.27
5 eV using the $(ah\nu)^2$ as a function of $h\nu$ (See Figure 4b). This result indicates that the
6 introduction of N-CQDs allows CaTiO₃ to be excited under the illumination of visible
7 light (>420 nm). This phenomenon can be rationalized by the up-conversion
8 fluorescence properties of N-CQDs that can emit light at shorter wavelength than the
9 excitation light. Consequently, when visible light was used as the excitation light, it
10 can be converted to UV light so that the CaTiO₃ can be excited^{33, 38}.

11
12
13 Photoelectrochemistry tests were carried out to probe the divorce of
14 photo-generated carriers. The transitory photocurrent generation over CaTiO₃/FTO
15 (Fluorine-doped tin oxide) and 3-N-CQDs/CaTiO₃/FTO electrodes was detected in
16 Na₂SO₃ solution under recurrent illumination of visible light at a wavelength of 420
17 nm. As shown in Figure 4c, the photocurrent response of CaTiO₃ is extremely weak
18 with the visible light being turned on whereas the photocurrent generated over
19 3-N-CQDs/CaTiO₃ is roughly 2.5 times larger than that over pure CaTiO₃. The result
20 implies that N-CQDs are capable of advancing the divorce of photo-generated carriers
21 over CaTiO₃, and eventually contribute to the larger photocurrent generation²⁵. The
22 electrons captured by O₂ on the surface of the 3-N-CQDs/CaTiO₃ and the reunion of
23 electrons and holes resulted in the loss of photocurrent (ΔI) during the irradiation
24 duration of visible light^{39, 40}. Intriguingly, ΔI weakened during recurrent irradiation
25 of visible light. This is because the amount of adsorbed O₂ on the surface of catalysts
26
27
28
29
30
31
32
33
34
35
36
37
38
39
40
41
42
43
44
45
46
47
48
49
50
51
52
53
54
55
56
57
58
59
60

1
2
3 decreased with the illumination time due to the limited diffusion of O₂ to the surface
4
5
6 of catalysts.
7

8 It was also noted the photocurrent is low even over N-CQDs/CaTiO₃. One of the
9
10 functions of N-CQDs is to promote the divorce of charge carrier in CaTiO₃. However,
11
12 the content of N-CQDs is very low (less than 1%) in N-CQDs/CaTiO₃, which may
13
14 lead to the limited promoting effects of N-CQDs on the separation of charge carrier.
15
16 On the other hand, up-conversion fluorescence properties of N-CQDs render N-CQDs
17
18 /CaTiO₃ excited by visible light. The weak absorption of visible light by low-content
19
20 N-CQDs may cause weak emission of UV light for the excitation of CaTiO₃, which
21
22 also rationalize the low photocurrent generated over N-CQDs /CaTiO₃ under visible
23
24 light irradiation.
25
26
27
28
29

30 **3.4. Photocatalytic activity and reaction mechanisms.** The energy band
31
32 structure plays a vital role in the activity of photocatalysts. The valence band position
33
34 is 2.46 eV based on the valence band (VB) XPS of CaTiO₃ (See Figure 4d). On the
35
36 basis of the formula $E_{CB} = E_{VB} - E_g$, and the band gap (E_g) of CaTiO₃ (3.27 eV), the
37
38 conduction band position (E_{CB}) of CaTiO₃ was determined to be -0.81 eV. In order to
39
40 confirm the band position of CaTiO₃, ESR spectroscopy was conducted to identify
41
42 hydroxyl radicals (DMPO-•OH) in CaTiO₃ aqueous suspension and superoxide
43
44 radicals (DMPO-O₂⁻) in CaTiO₃ methanol suspension under UV irradiation. As
45
46 shown in the Figure S3, CaTiO₃ can produce the •O₂⁻ and •OH under UV
47
48 irradiation, suggesting the CB potential negative to the redox potential of O₂/•
49
50 O₂⁻ (-0.33 eV) and the VB potential positive to the H₂O/•OH (2.37 eV)⁴¹, implying the
51
52
53
54
55
56
57
58
59
60

1
2
3
4 calculated band positions of CaTiO_3 was reasonable in this study. Mizoguchi et al.
5
6 reported the CB potential was -0.78 eV which similar to that in our study⁴². It was
7
8 observed the addition of PEG could red shift the light absorption of the material so
9
10 that the band gap was narrowed to the 3.27 eV⁴³.

11
12
13 It was reported that the presence of carbonaceous materials promote the adsorption
14
15 of dye on the TiO_2 ⁴⁴. To evaluate the influence the introduction of N-CQDs on the
16
17 adsorption ability of CaTiO_3 , TGA and NO-TPD were conducted to explore the
18
19 interaction between NO and the as-synthesized photocatalysts. The TGA curve of
20
21 samples shows three weight loss stages (See Figure 5a). It is worth noting that in the
22
23 third stage above 580°C , the curve of pure CaTiO_3 has no change, and the mass loss
24
25 of N-CQDs/ CaTiO_3 linearly correlated with the N-CQDs contents. It can be
26
27 concluded that N-CQDs are decomposed above 580°C . It is also intriguing to notice
28
29 that the whole weight loss of 5-N-CQDs/ CaTiO_3 is more than 15%, indicating that the
30
31 addition of 0.5 mL N-CQDs will change the crystal of CaTiO_3 which lead to the
32
33 difference of photocatalytic activity (See Figure S1). Figure 5b shows that pure
34
35 CaTiO_3 has two discernible desorption peaks, the peak at around 350°C coming from
36
37 the desorption of NO (N-CQDs will decomposed above 580°C), and the one at 630
38
39 $^\circ\text{C}$ deriving from the release of O_2 from the CaTiO_3 lattice⁴⁵. This suggests that NO
40
41 can be chemically adsorbed onto CaTiO_3 surface at ambient temperature. The NO
42
43 desorption as a function of temperature is also presented over the 3-N-CQDs/ CaTiO_3 .
44
45
46
47
48
49
50
51
52 In contrast to CaTiO_3 , NO desorption temperature shifted to 450°C over
53
54 3-N-CQDs/ CaTiO_3 , indicating the enhanced adsorption capacity of
55
56
57
58
59
60

1
2
3 3-N-CQDs/CaTiO₃. It can be concluded that the N-CQDs may have the potential to
4
5 increase the adsorption ability of CaTiO₃.
6
7

8 Based on the aforementioned results, the introduction of N-CQDs can broaden the
9
10 optical response range to allow CaTiO₃ being excited by visible light. The intrinsic
11
12 electron storage capacity of N-CQDs allows the efficient divorcement of the
13
14 photogenerated carriers. The N-CQDs can enhance the adsorption ability for NO
15
16 which would fundamentally boost the photocatalytic performances.
17
18
19

20 The visible light-driven photocatalytic activities of CaTiO₃ and N-CQDs/CaTiO₃
21
22 composites were gauged in terms of the photocatalytic elimination of NO_x. As
23
24 illustrated in Figure 6a, the NO removal efficiency was enhanced when N-CQDs dose
25
26 being escalated. The best performance was achieved over 3-N-CQDs/CaTiO₃, where
27
28 the concentration of nitrogen oxide at the outlet decreased 25% in comparison with
29
30 that at the inlet removed after 0.5 h. The decrease of NO_x concentration is almost 5
31
32 times larger than that over CaTiO₃ (5%) and apparently larger than that over P25
33
34 (14%). No significant deactivation was observed in 30 min. With the further
35
36 increment of N-CQDs dose, the photocatalytic activity of 5-N-CQDs/CaTiO₃
37
38 decreased although 5-N-CQDs/CaTiO₃ has the strongest visible light absorption. The
39
40 higher N-CQDs content made CaTiO₃ agglomerate as shown in Figure S1, leading to
41
42 less active sites available for NO adsorption. The concentration of NO₂ in the outlet
43
44 gas was concurrently detected. The NO removal efficiency (C_0-C/C_0) and NO₂
45
46 conversion ratio ($\Delta\text{NO}_2/(C_0-C)$) over different samples are presented in Figure 6b.
47
48
49
50
51
52
53
54
55
56
57
58
59
60

1
2
3 The 3-N-CQDs/CaTiO₃ composite shows superior performance in terms of NO₂ yield
4 (9.6%), which is lower than that over pure CaTiO₃ (104.3%) .
5
6

7
8 The stability of the 3-N-CQDs/CaTiO₃ composite was examined by the repeated
9 photocatalytic experiments under identical conditions (See Figure S2). The NO
10 removal efficiency decreased to 16% after 3-N-CQDs/CaTiO₃ being recycled for 5
11 times, implying that the catalyst is relatively unstable. However, being washed by
12 deionized water can restore the photocatalytic activity of 3-N-CQDs/CaTiO₃, which
13 can be rationalized by the elimination of NO oxidation products including NO₃⁻ and
14 NO₂⁻ on the catalyst surface. The concentration of nitrate and nitrite ions on the
15 surface of CaTiO₃ and 3-N-CQDs/CaTiO₃ after single run reaction was detected and
16 shown in Table S1. NO₃⁻ generated on 3-N-CQDs/CaTiO₃ surfaces was quantified to
17 be 57.28 μg/m², which is 1.46 times as high as that generated on the CaTiO₃ (39.29
18 μg/m²), implying that the presence of N-CQDs shifted the photocatalytic reaction on
19 CaTiO₃ surface towards the yield of nitrate formation. Besides, the generation of trace
20 NO₂⁻ was observed.
21
22
23
24
25
26
27
28
29
30
31
32
33
34
35
36
37
38
39

40 ESR spectroscopy was conducted to determine the reactive radicals participating
41 in photocatalytic oxidation of NO over CaTiO₃ and 3-N-CQDs/CaTiO₃ under visible
42 light illumination. Figure 6c-d shows no signal in the case of CaTiO₃, indicating
43 neither •O₂⁻ nor •OH radicals were generated. Both the typical DMPO-•O₂⁻ and
44 DMPO-•OH signals were strong in the case of the 3-N-CQDs/CaTiO₃ sample.
45
46
47
48
49
50
51

52 The photocatalytic reaction process for the NO degradation over N-CQDs/CaTiO₃
53 composite was described in Figure 7. Under the irradiation of visible light, the
54
55
56
57
58
59
60

1
2
3 N-CQDs adsorb visible light, and then radiate UV light owing to up-conversion
4
5 effects, which in turn excite CaTiO₃ to spawn electron and hole pairs. The carbon
6
7 nanomaterials have the potential to accept and transport electrons, which favored the
8
9 electrons being transferred from CB of CaTiO₃ to N-CQDs and accumulating on the
10
11 N-CQDs. As a result, electrons-holes pairs were separated efficiently. In addition, the
12
13 introduction of N-CQDs promoted NO adsorption over CaTiO₃, which is also
14
15 beneficial for oxidation reaction of NO.
16
17
18
19

20 The whole process of photocatalytic NO removal over the N-CQDs/CaTiO₃
21
22 composite under visible light are described as the following:
23
24



32 33 34 35 36 37 38 39 40 41 42 43 44 45 46 47 48 49 50 51 52 53 54 55 56 57 58 59 60

46 In brief, a facile hydrothermal method was used to construct N-CQDs/CaTiO₃
47
48 composite photocatalyst. In contrast with CaTiO₃ and P25, the composite exhibits
49
50 increased visible light-induced photocatalytic activity in respect of NO degradation
51
52 and lower selectivity towards NO₂ formation. The N-CQDs are believed to play
53
54 multiple roles including wavelength converter, electron reservoir and transporter as
55
56
57
58
59
60

1
2
3 well as an excellent NO_x adsorber during the photocatalytic oxidation of NO over
4
5 N-CQDs/CaTiO₃; the synergistic effects of these multiple roles account for the
6
7 superior photocatalytic capacity of N-CQDs/CaTiO₃.
8
9

10 **ASSOCIATED CONTENT**

11 **Supporting Information**

12
13 The Supporting Information is available free of charge on the ACS Publications
14
15 website.
16
17

18
19 Figure for SEM images of every catalysts, figure for the cyclic NO degradation tests,
20
21 figure for DMPO spin-trapping ESR spectra of CaTiO₃ under UV light illumination,
22
23 table for the BET specific surface area and the amount of nitrate and nitrite
24
25 accumulated on the surface of CaTiO₃ and 3-N-CQDs/CaTiO₃ (PDF).
26
27
28
29
30

31 **ACKNOWLEDGMENTS**

32
33 This work was financially supported by “State Key Laboratory of Loess and
34
35 Quaternary Geology, Institute of Earth Environment, CAS (No. SKLLQG1516)” and
36
37 “Key Laboratory of Aerosol Chemistry and Physics, Institute of Earth Environment,
38
39 CAS (No. KLACP1701)”
40
41
42
43

44 **REFERENCES**

- 45
46 1. Zhao, B.; Wang, S. X.; Liu, H.; Xu, J. Y.; Fu, K.; Klimont, Z.; Hao, J. M.; He, K. B.; Cofala, J.;
47
48 Amann, M., NO_x emissions in China: historical trends and future perspectives. *Atmospheric Chemistry*
49
50 *& Physics* **2013**, 13 (19), 9869-9897.
51
52
53 2. Bilgen, S., Structure and environmental impact of global energy consumption. *Renewable &*
54
55 *Sustainable Energy Reviews* **2014**, 38, 890-902.
56
57
58
59
60

- 1
2
3
4 3. Zhao, B.; Liou, K. N.; Gu, Y.; Li, Q. B.; Jiang, J. H.; Su, H.; He, C. L.; Tseng, H. L. R.; Wang, S.
5
6 X.; Liu, R.; Qi, L.; Lee, W. L.; Hao, J. M., Enhanced PM_{2.5} pollution in China due to aerosol-cloud
7
8 interactions. *Scientific Reports* **2017**, *7*, 1-11.
9
10
11 4. Huang, R. J.; Zhang, Y.; Bozzetti, C.; Ho, K. F.; Cao, J. J.; Han, Y.; Daellenbach, K. R.; Slowik,
12
13 J. G.; Platt, S. M.; Canonaco, F., High secondary aerosol contribution to particulate pollution during
14
15 haze events in China. *Nature* **2014**, *514* (7521), 218-22.
16
17
18 5. Quan, J. N.; Liu, Q.; Li, X.; Gao, Y.; Jia, X. C.; Sheng, J. J.; Liu, Y. G., Effect of heterogeneous
19
20 aqueous reactions on the secondary formation of inorganic aerosols during haze events. *Atmospheric*
21
22 *Environment* **2015**, *122*, 306-312.
23
24
25 6. Song, C. B.; Wu, L.; Xie, Y. C.; He, J. J.; Chen, X.; Wang, T.; Lin, Y. C.; Jin, T. S.; Wang, A. X. ;
26
27 Liu, Y.; Dai, Q. L.; Liu, B. S.; Wang, Y. N.; Mao, H. J., Air pollution in China: Status and
28
29 spatiotemporal variations. *Environmental Pollution* **2017**, *227*, 334-347.
30
31
32
33 7. Granger, P.; Parvulescu, V. I., Catalytic NO(x) abatement systems for mobile sources: from
34
35 three-way to lean burn after-treatment technologies. *Chemical Reviews* **2011**, *111* (5), 3155-3207.
36
37
38 8. Macleod, N.; Cropley, R.; Keel, J. M.; Lambert, R. M., Exploiting the synergy of titania and
39
40 alumina in lean NO_x reduction: in situ ammonia generation during the Pd/TiO₂/Al₂O₃ -catalysed H₂
41
42 /CO/NO/O₂ reaction. *Journal of Catalysis* **2004**, *221* (1), 20-31.
43
44
45 9. Tanaka, T.; Teramura, K.; Arakaki, K.; Funabiki, T., Photoassisted NO reduction with NH₃ over
46
47 TiO₂ photocatalyst. *Chemical Communications* **2002**, *22* (22), 2742-2743.
48
49
50 10. Schneider, J.; Matsuoka, M.; Takeuchi, M.; Zhang, J.; Horiuchi, Y.; Anpo, M.; Bahnemann, D.
51
52 W., Understanding TiO₂ photocatalysis: mechanisms and materials. *Chemical Reviews* **2014**, *114* (19),
53
54 9919-9986.
55
56
57
58
59
60

- 1
2
3
4
5
6
7
8
9
10
11
12
13
14
15
16
17
18
19
20
21
22
23
24
25
26
27
28
29
30
31
32
33
34
35
36
37
38
39
40
41
42
43
44
45
46
47
48
49
50
51
52
53
54
55
56
57
58
59
60
11. Hoffmann, M. R.; Martin, S. T.; Choi, W.; Bahnemann, D. W., Environmental Applications of Semiconductor Photocatalysis. *Chemical Reviews* **1995**, 95 (1), 69-96.
12. Boyjoo, Y.; Su, H.; Liu, J.; Pareek, V. K.; Wang, S., A review on photocatalysis for air treatment: From catalyst development to reactor design. *Chemical Engineering Journal* **2017**, 310, 537-559.
13. Tanaka, H.; Misono, M., Advances in designing perovskite catalysts. *Current Opinion in Solid State & Materials Science* **2001**, 5 (5), 381-387.
14. Zhu, J.; Thomas, A., Perovskite-type mixed oxides as catalytic material for NO removal. *Applied Catalysis B-Environmental* **2009**, 92 (3-4), 225-233.
15. Zhang, Q.; Huang, Y.; Xu, L.; Cao, J.-j.; Ho, W.; Lee, S. C., Visible-Light-Active Plasmonic Ag-SrTiO₃ Nanocomposites for the Degradation of NO in Air with High Selectivity. *ACS Appl Mater Interfaces* **2016**, 8 (6), 4165-4174.
16. Grabowska, E., Selected perovskite oxides: Characterization, preparation and photocatalytic properties-A review. *Applied Catalysis B-Environmental* **2016**, 186, 97-126.
17. Alammar, T.; Hamm, I.; Wark, M.; Mudringad, A. V., Low-temperature route to metal titanate perovskite nanoparticles for photocatalytic applications. *Applied Catalysis B-Environmental* **2015**, 178, 20-28.
18. Lozano-Sánchez, L. M.; Méndez-Medrano, M. G.; Colbeau-Justin, C.; Rodríguez-López, J. L.; Hernández-Uresti, D. B.; Obregón, S., Long-lived photoinduced charge-carriers in Er³⁺ doped CaTiO₃ for photocatalytic H₂ production under UV irradiation. *Catalysis Communications* **2016**, 84, 36-39.
19. Han, C.; Liu, J.; Yang, W.; Wu, Q.; Yang, H.; Xue, X., Photocatalytic activity of CaTiO₃ synthesized by solid state, sol-gel and hydrothermal methods. *Journal of Sol-Gel Science and Technology* **2017**, 81 (3), 806-813.

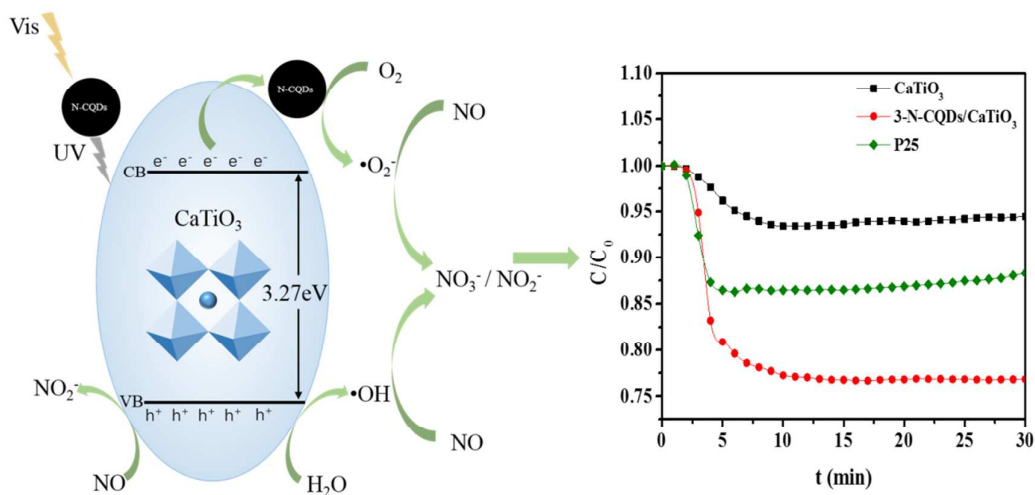
- 1
2
3
4 20. Huang, X.-j.; Yan, X.; Wu, H.-y.; Fang, Y.; Min, Y.-h.; Li, W.-s.; Wang, S.-y.; Wu, Z.-j.,
5 Preparation of Zr-doped CaTiO₃ with enhanced charge separation efficiency and photocatalytic
6 activity. *Transactions of Nonferrous Metals Society of China* **2016**, 26 (2), 464-471.
7
8
9
10 21. Han, C.; Liu, J.; Yang, W.; Wu, Q.; Yang, H.; Xue, X., Enhancement of photocatalytic activity of
11 CaTiO₃ through HNO₃ acidification. *Journal of Photochemistry and Photobiology A: Chemistry* **2016**,
12 322-323, 1-9.
13
14
15
16
17 22. Nishimoto, S.; Matsuda, M.; Miyake, M., Photocatalytic activities of rh-doped CaTiO₃ under
18 visible light irradiation. *Chemistry Letters* **2006**, 35 (3), 308-309.
19
20
21
22 23. Lim, S. Y.; Shen, W.; Gao, Z., Carbon quantum dots and their applications. *Chemical Society*
23 *Reviews* **2015**, 44 (1), 362-381.
24
25
26
27 24. Duo, F.; Wang, Y.; Fan, C.; Zhang, X.; Wang, Y., Enhanced visible light photocatalytic activity
28 and stability of CQDs/BiOBr composites: The upconversion effect of CQDs. *Journal of Alloys and*
29 *Compounds* **2016**, 685, 34-41.
30
31
32
33
34 25. Huang, Y.; Liang, Y.; Rao, Y.; Zhu, D.; Cao, J. J.; Shen, Z.; Ho, W.; Lee, S. C.,
35 Environment-Friendly Carbon Quantum Dots/ZnFe₂O₄ Photocatalysts: Characterization,
36 Biocompatibility, and Mechanisms for NO Removal. *Environmental Science & Technology* **2017**, 51
37 (5), 2924-2933.
38
39
40
41
42 26. Ji, M.; Xia, J.; Di, J.; Wang, B.; Sheng, Y.; Li, X.; Zhao, J.; Li, H., Ionic Liquid-Assisted
43 Bidirectional Regulation Strategy for Carbon Quantum Dots (CQDs)/Bi₄O₅I₂ Nanomaterials and
44 Enhanced Photocatalytic Properties. *Journal of Colloid & Interface Science* **2016**, 478, 324-333.
45
46
47
48 27. Zhang, H.; Huang, H.; Ming, H.; Li, H.; Zhang, L.; Liu, Y.; Kang, Z., Carbon quantum
49 dots/Ag₃PO₄ complex photocatalysts with enhanced photocatalytic activity and stability under visible
50 light. *Journal of Materials Chemistry* **2012**, 22 (21), 10501-10506.
51
52
53
54
55
56
57
58
59
60

- 1
2
3
4 28. Zhang, P.; Song, T.; Wang, T.; Zeng, H., In-situ synthesis of Cu nanoparticles hybridized with
5 carbon quantum dots as a broad spectrum photocatalyst for improvement of photocatalytic H₂
6 evolution. *Applied Catalysis B-Environmental* **2017**, 206, 328-335.
7
8
9
10 29. Zhang, Y.; Jing, N.; Zhang, J.; Wang, Y., Hydrothermal synthesis of nitrogen-doped carbon dots
11 as a sensitive fluorescent probe for the rapid, selective determination of Hg²⁺. *International Journal of*
12 *Environmental Analytical Chemistry* **2017**, 97 (9), 841-853.
13
14
15
16
17 30. Sopha, H.; Krbal, M.; Ng, S.; Prikryl, J.; Zazpe, R.; Yam, F. K.; Macak, J. M., Highly efficient
18 photoelectrochemical and photocatalytic anodic TiO₂ nanotube layers with additional TiO₂ coating.
19
20
21 *Applied Materials Today* **2017**, 9, 104-110.
22
23
24 31. Zhang, Y.-Q.; Ma, D.-K.; Zhang, Y.-G.; Chen, W.; Huang, S.-M., N-doped carbon quantum dots
25 for TiO₂-based photocatalysts and dye-sensitized solar cells. *Nano Energy* **2013**, 2 (5), 545-552.
26
27
28
29 32. Martins, N. C. T.; Ângelo, J.; Girão, A. V.; Trindade, T.; Andrade, L.; Mendes, A., N-doped
30 carbon quantum dots/TiO₂ composite with improved photocatalytic activity. *Applied Catalysis B:*
31 *Environmental* **2016**, 193, 67-74.
32
33
34
35
36 33. Zhang, Y.; Park, M.; Kim, H. Y.; Ding, B.; Park, S. J., A facile ultrasonic-assisted fabrication of
37 nitrogen-doped carbon dots/BiOBr up-conversion nanocomposites for visible light photocatalytic
38 enhancements. *Scientific Reports* **2017**, 7, 1-12.
39
40
41
42 34. Wang, F.; Chen, P.; Feng, Y.; Xie, Z.; Liu, Y.; Su, Y.; Zhang, Q.; Wang, Y.; Yao, K.; Lv, W.;
43 Liu, G., Facile synthesis of N-doped carbon dots/g-C₃N₄ photocatalyst with enhanced visible-light
44 photocatalytic activity for the degradation of indomethacin. *Applied Catalysis B-Environmental* **2017**,
45 207, 103-113.
46
47
48
49
50
51
52
53
54
55
56
57
58
59
60

- 1
2
3
4 35. Wei, J.; Li, X.-D.; Wang, H.-Z.; Zhang, Q.-H.; Li, Y.-G., Nitrogen Doped Carbon Quantum
5
6 Dots/Titanium Dioxide Composites for Hydrogen Evolution under Sunlight. *Journal of Inorganic*
7
8 *Materials* **2015**, 30 (9), 925-930.
9
- 10
11 36. Gao, Y.; Huang, Y.; Li, Y.; Zhang, Q.; Cao, J.-j.; Ho, W.; Lee, S. C., Plasmonic Bi/ZnWO₄
12
13 Microspheres with Improved Photocatalytic Activity on NO Removal under Visible Light. *ACS*
14
15 *Sustainable Chemistry & Engineering* **2016**, 4 (12), 6912-6920.
16
17
- 18 37. Chen, Q.; Wang, Y.; Wang, Y.; Zhang, X.; Duan, D.; Fan, C., Nitrogen-doped carbon quantum
19
20 dots/Ag₃PO₄ complex photocatalysts with enhanced visible light driven photocatalytic activity and
21
22 stability. *Journal of Colloid and Interface Science* **2017**, 491, 238-245.
23
- 24 38. Wang, H.; Sun, P.; Cong, S.; Wu, J.; Gao, L.; Wang, Y.; Dai, X.; Yi, Q.; Zou, G., Nitrogen-Doped
25
26 Carbon Dots for "green" Quantum Dot Solar Cells. *Nanoscale Research Letters* **2016**, 11, 27-32.
27
28
- 29 39. Yen, Y. C.; Lin, C. C.; Chen, P. Y.; Ko, W. Y.; Tien, T. R.; Lin, K. J., Green synthesis of carbon
30
31 quantum dots embedded onto titanium dioxide nanowires for enhancing photocurrent. *Royal Society*
32
33 *Open Science* **2017**, 4 (5), 1-9.
34
35
- 36 40. Yang, D.; Feng, J.; Jiang, L.; Wu, X.; Sheng, L.; Jiang, Y.; Wei, T.; Fan, Z., Photocatalyst
37
38 Interface Engineering: Spatially Confined Growth of ZnFe₂O₄ within Graphene Networks as Excellent
39
40 Visible-Light-Driven Photocatalysts. *Advanced Functional Materials* **2015**, 25 (45), 7080-7087.
41
42
- 43 41. Wang, Z.; Huang, Y.; Ho, W.; Cao, J.; Shen, Z.; Lee, S. C., Fabrication of Bi₂O₂CO₃ /g-C₃N₄
44
45 heterojunctions for efficiently photocatalytic NO in air removal: In-situ self-sacrificial synthesis,
46
47 characterizations and mechanistic study. *Applied Catalysis B: Environmental* **2016**, 199, 123-133.
48
- 49 42. Mizoguchi, H.; Ueda, K.; Orita, M.; Moon, S. C.; Kajihara, K.; Hirano, M.; Hosono, H.,
50
51 Decomposition of water by a CaTiO₃ photocatalyst under UV light irradiation. *Materials Research*
52
53 *Bulletin* **2002**, 37 (15), 2401-2406.
54
55
56
57
58
59
60

- 1
2
3
4 43. Luevano-Hipolito, E.; Martinez-de la Cruz, A.; Yu, Q. L.; Brouwers, H. J. H., Precipitation
5
6 synthesis of WO₃ for NO_x using PEG as template. *Ceramics International* **2014**, 40 (8), 12123-12128.
7
8
9 44. Pu, S.; Zhu, R.; Ma, H.; Deng, D.; Pei, X.; Qi, F.; Chu, W., Facile in-situ design strategy to
10
11 disperse TiO₂ nanoparticles on graphene for the enhanced photocatalytic degradation of rhodamine 6G.
12
13 *Applied Catalysis B-Environmental* **2017**, 218, 208-219.
14
15
16 45. Zhang, Q.; Huang, Y.; Peng, S.; Zhang, Y.; Shen, Z.; Cao, J.-j.; Ho, W.; Lee, S. C.; Pui, D. Y. H.,
17
18 Perovskite LaFeO₃ -SrTiO₃ composite for synergistically enhanced NO removal under visible light
19
20 excitation. *Applied Catalysis B: Environmental* **2017**, 204, 346-357.
21
22
23
24
25
26
27
28
29
30
31
32
33
34
35
36
37
38
39
40
41
42
43
44
45
46
47
48
49
50
51
52
53
54
55
56
57
58
59
60

TOC graphic



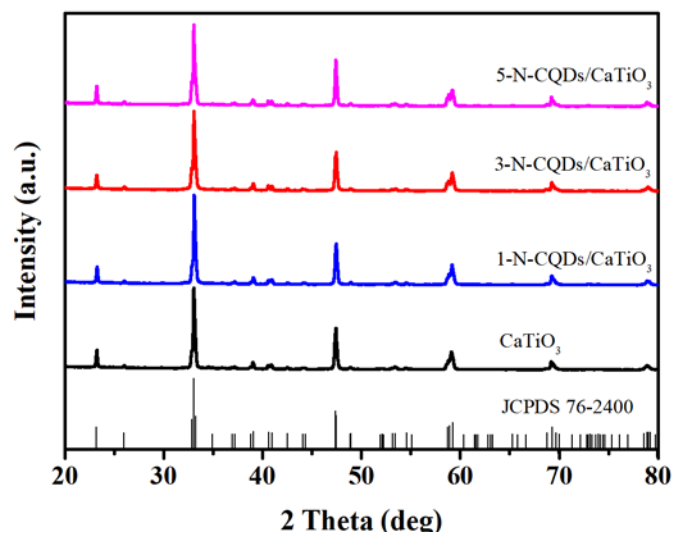


Figure 1. Powder XRD patterns of pure CaTiO₃ and N-CQDs nanocomposites with various N-CQDs loading amount

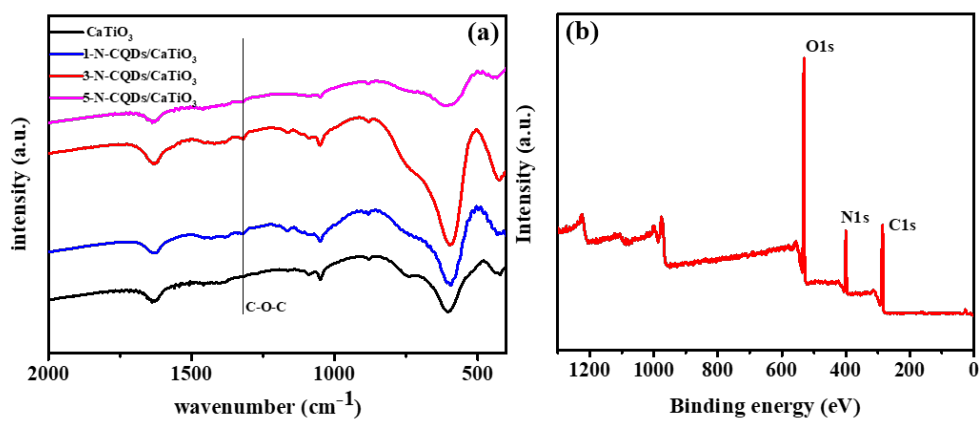


Figure 2. (a) FT-IR spectra of as-prepared samples; (b) Survey XPS spectra of N-CQDs

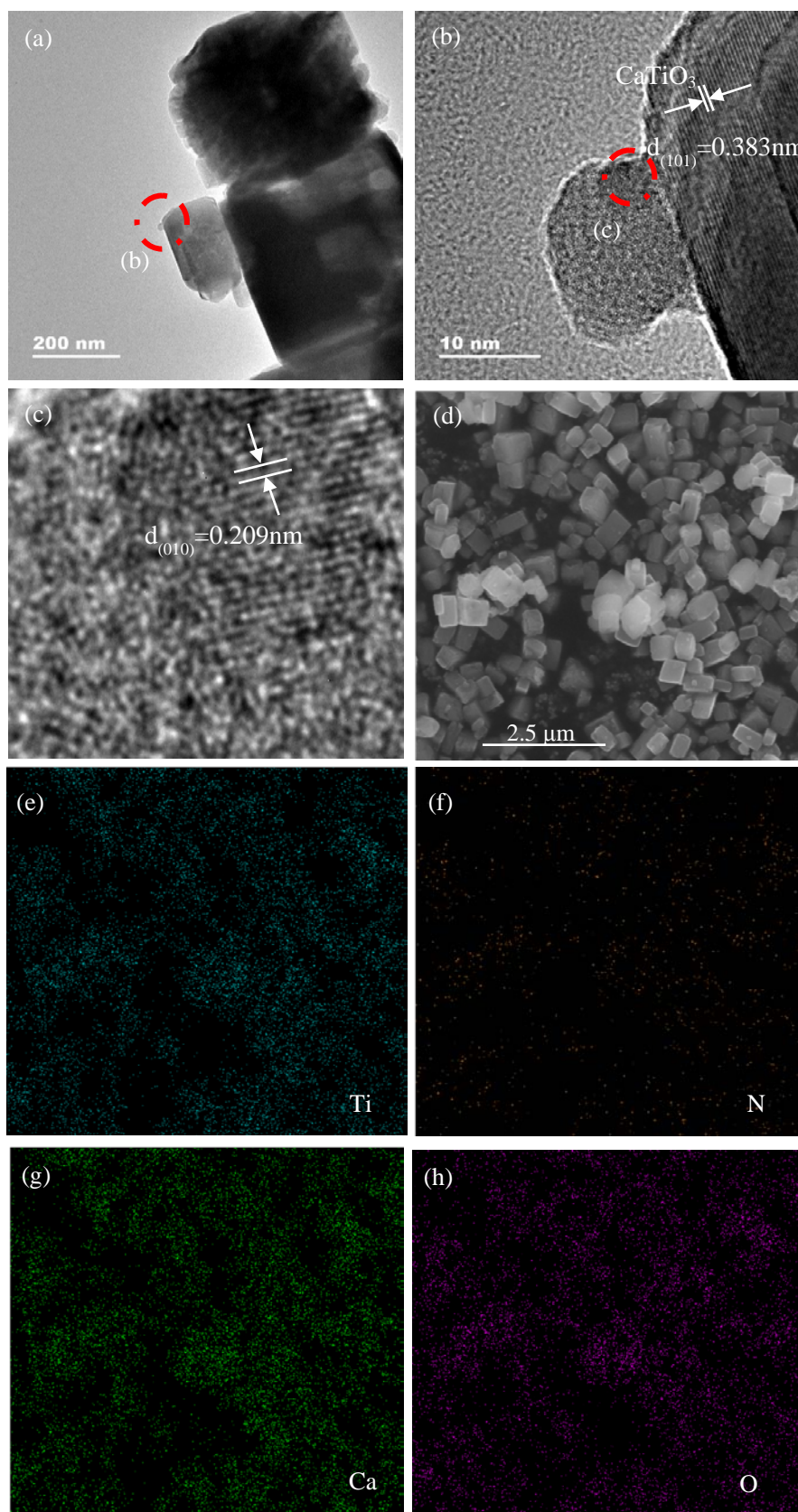


Figure 3. (a-c) HRTEM images of 3-N-CQDs/CaTiO₃ and; (d) SEM images of the 3-N-CQDs/CaTiO₃; (e-h) representative the EDX mapping images corresponding to (d)

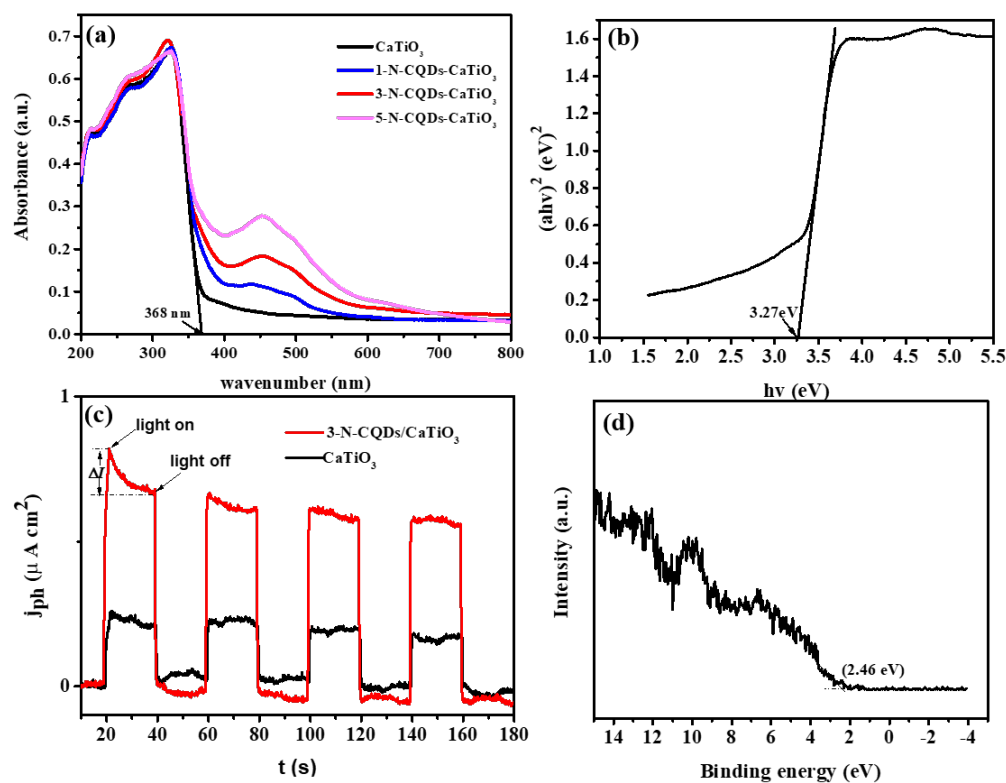


Figure 4. (a) UV-visible diffuse reflectance spectra of CaTiO₃ and N-CQDs/CaTiO₃; (b) $(\alpha h\nu)^2$ vs $h\nu$ of CaTiO₃; (c) Photocurrent responses of CaTiO₃ and 3-N-CQDs/CaTiO₃ in 0.5 M Na₂SO₃ electrolyte under visible light irradiation ($\lambda = 420$ nm); (d) valence band XPS spectra of pure CaTiO₃

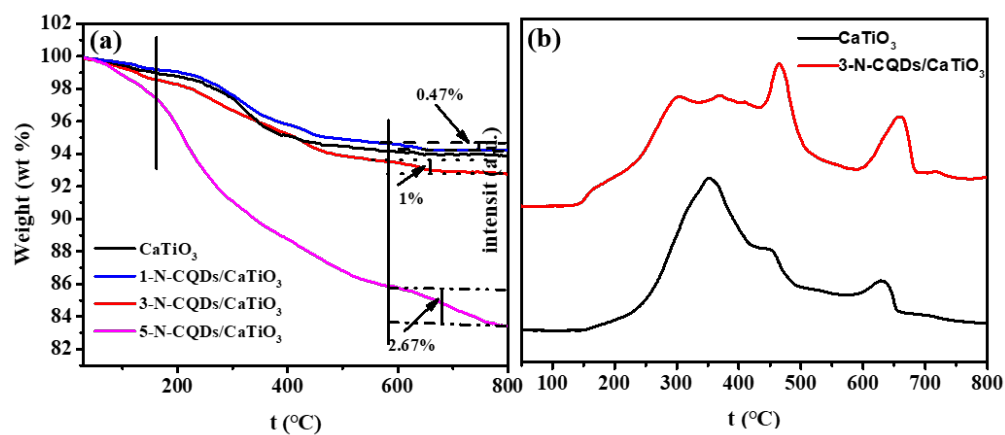


Figure 5. (a) TGA of CaTiO₃ and N-CQDs/CaTiO₃; (b) TPD profiles of NO for the as-prepared pristine CaTiO₃ and 3-N-CQDs/CaTiO₃

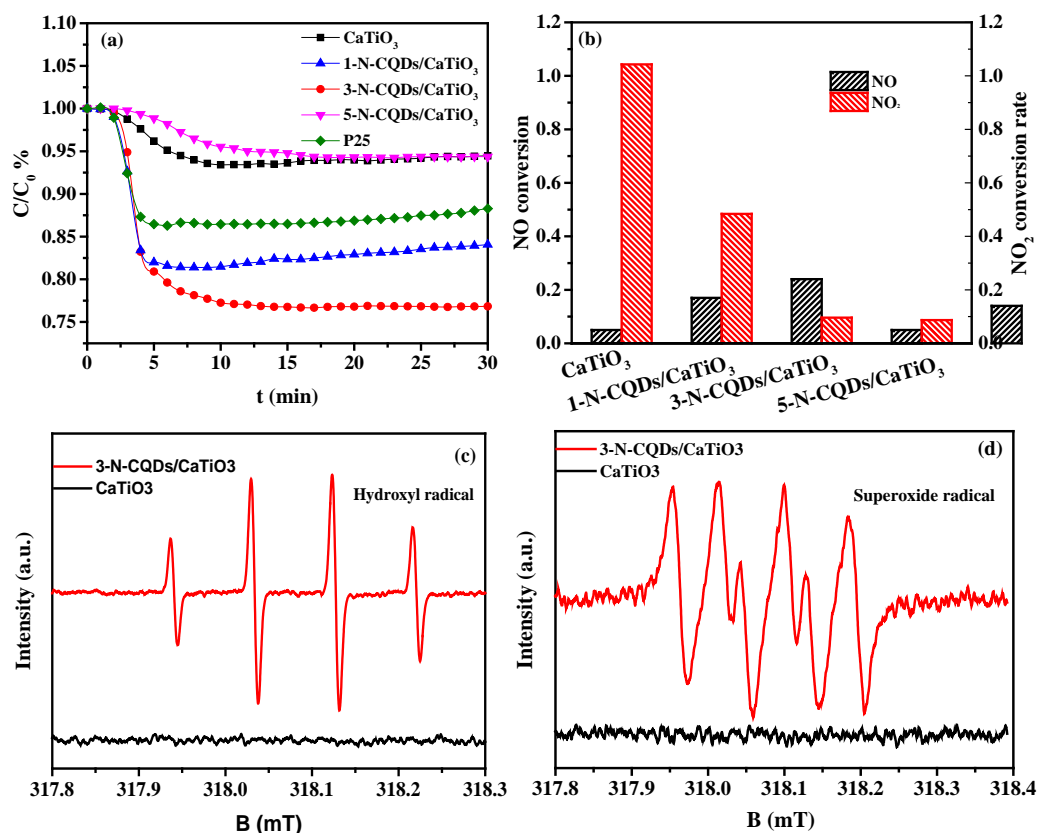


Figure 6. (a) Visible light photocatalytic removal of NO (b) Comparison of the NO conversion rate (C/C_0) and NO₂ conversion rate over CaTiO₃, N-CQDs/CaTiO₃ and P25; (c, d) DMPO spin-trapping ESR spectra of CaTiO₃ and 3-N-CQDs/CaTiO₃ in aqueous dispersion for DMPO-•OH and in methanol dispersion for DMPO-•O₂⁻ under illumination for 12 min ($\lambda \cong 420$ nm)

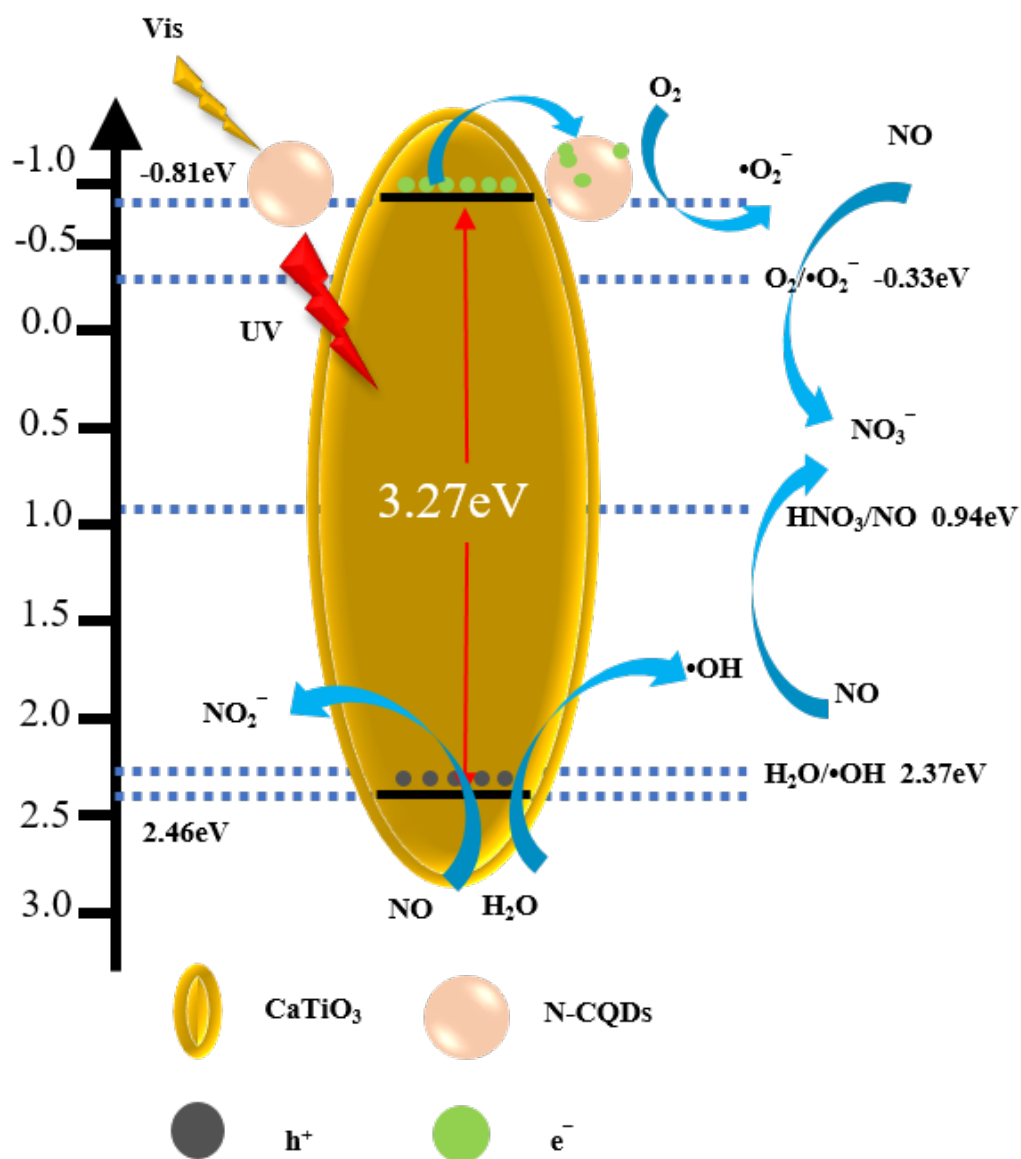


Figure 7. Proposed photocatalytic mechanism for enhancing photocatalytic activity over 3-N-CQDs/CaTiO₃ composite under visible light irradiation